


A. DI FALCO  
C. CONTI  
G. ASSANTO 

# Photonic crystal wires for optical parametric oscillators in isotropic media

NOOEL-Nonlinear Optics and OptoElectronics Laboratory, National Institute for the Physics of the Matter (INFN), University “Roma Tre”, Via della Vasca Navale 84, 00186 Rome, Italy

Received: 12 February 2004/  
Revised version: 18 February 2004  
Published online: 7 April 2004 • © Springer-Verlag 2004

**ABSTRACT** We investigate four wave mixing in photonic crystal wire microresonators realized in an isotropic medium. One-dimensional optical parametric oscillators are numerically analyzed by solving Maxwell’s equations in all dimensions and including material dispersion as well as nonlinear polarization.

**PACS** 42.65.Yj; 42.70.Qs; 42.82.Gw

## 1 Introduction

The interest of photonic crystals (PC) relies mostly on the design versatility afforded by such structures in various materials for use in micro- and nano-optics and integrated applications. The engineering of the dispersion relation in PC-based devices can be achieved by periodic alternation of high and low refractive index materials in one, two or three dimensions, and has been extensively studied and demonstrated [1–4]. Several linear and nonlinear phenomena have been proposed for exploitation in PC structures, spanning from Bragg reflectors and bistable gates to filters, delay lines, waveguides, switches, lasers [5–11]. In the past few years, by introducing suitably located defects in the periodic pattern, researchers have been able to obtain high quality ( $Q$ -) factors for the modes resonating in PC structures, up to values  $Q > 10^4$  [12]. More recently, the features of optical modes near the band-edges have been examined in two dimensional (2D-) PC exhibiting comparably high  $Q$ -factors [13].

One of the simplest PC geometries is the PC-wire, i.e., a strip of material with a limited number of holes able to open a band-gap in the transmission characteristic. Among them, air-bridge PC-wires are particularly interesting and potentially amenable to the highest degree of circuit integration [14].

In this paper we show for the first time how the micro-resonant structure of an air-bridge PC-wire can be exploited to efficiently confine light and obtain gain and optical parametric oscillation of the cavity modes via four wave mixing (FWM), exploiting the cubic response of isotropic media.

In the next section we describe the model and its numerical implementation, while in Sect. 3 we perform the modal analysis of the structure. Finally, in Sect. 4 we explore the oscillatory behaviour of the PC-wire subject to high power pumping. We will show how the oscillation dynamics relates to the pumped mode, in terms of both symmetry constraints and quality factors.

## 2 Numerical Model

Optical oscillations throughout energy exchange between PC modes via nonlinear four wave mixing can be studied by means of a finite-difference time-domain (FDTD) code. Maxwell’s equations were solved with no approximations, except for discretization, in both the three spatial coordinates and time. An isotropic nonlinear medium was modeled by introducing a Lorentz oscillator yielding the cubic polarization  $\mathbf{P}$ :

$$\begin{aligned}\nabla \times \mathbf{E} &= -\mu_0 \frac{\partial \mathbf{H}}{\partial t} \\ \nabla \times \mathbf{H} &= \varepsilon_0 \frac{\partial \mathbf{E}}{\partial t} + \frac{\partial \mathbf{P}}{\partial t} \\ \frac{\partial^2 \mathbf{P}}{\partial t^2} + 2\gamma_0 \frac{\partial \mathbf{P}}{\partial t} + \omega_0^2 f(P) \mathbf{P} &= \varepsilon_0 (\varepsilon_s - 1) \hat{\omega}_0^2 \mathbf{E}\end{aligned}\quad (1)$$

where  $f(P) = 1$  ( $P^2 = \mathbf{P} \cdot \mathbf{P}$ ) represents a linear single-pole dispersive response. To describe an isotropic Kerr-like material we chose  $f(P) = [1 + (P/P_0)^2]^{-3/2}$  as in [15]. As long as the ratio  $P/P_0$  is small, a standard Kerr response is retrieved; as its size becomes appreciable, however, the model is able to account for higher order terms ( $\chi^{(5)}$  etc.). For the integration we employed a nonlinear generalization of the L-DIM1 approach for dispersive media [16]. To enforce electromagnetic field continuity at the boundaries between different media and prevent spurious reflections, we adopted the Yee’s grid and uniaxial perfectly matched layers (UPML) [17]. The sourcing was arranged throughout a total-field/scattered-field (TF/SF) approach, allowing both single-cycle (SC) and continuous wave (cw) excitations, the latter mimicked by an “*mn*m” pulse. The “*mn*m” pulse allows for the avoiding of undesired spectral distortions by trailing and tailing with  $m$  cycles while holding the peak value for  $n$  cycles, respectively [18]. A linear waveguide provided the input to the nonlinear portion of the

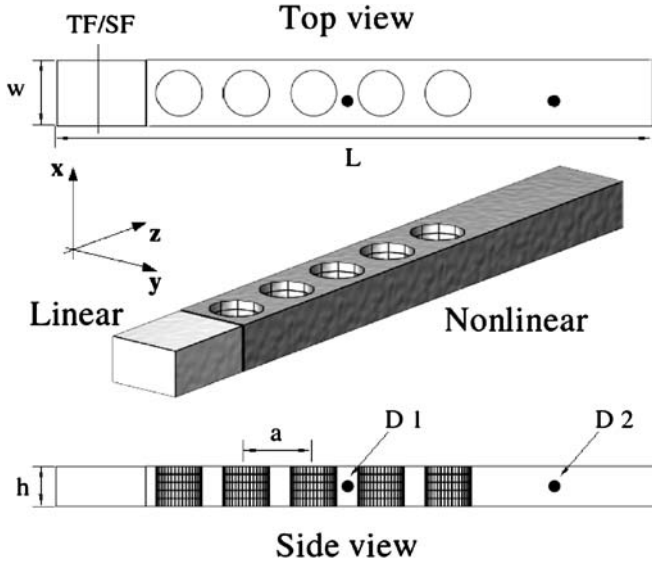


**FIGURE 1** Sketch of the structure. In the *top panel*, TF/SF indicates the sourcing interface, D1 and D2 the photodetectors,  $a$  the PC lattice constant

structure. Such an in-coupling arrangement not only preserves the validity of the TF/SF implementation, but also effectively holds the adopted UPML boundaries even at high fluencies, when an index change could alter the invariance of the refractive distribution [17].

Figure 1 is a sketch of the geometry: a one-dimensional photonic crystal contains holes of radius  $0.35a$ , with  $a = 450$  nm the PC lattice constant (i.e., the distance between neighboring holes). The  $4 \mu\text{m}$ -long strip,  $450$  nm wide and  $270$  nm thick, ensures single-mode propagation in the input waveguide and throughout the frequency range of relevance. D1 and D2 indicate the placement of virtual photodetectors to monitor electric fields and powers. The entire simulation window was sized  $4 \times 1.2 \times 1.2 \mu\text{m}^3$ , and the spatial discretization provided  $\Delta x = \Delta y = 20$  nm and  $\Delta z \simeq 16$  nm. The time-step was set to  $\Delta t = 0.008$  fs. For the parameters of the Lorentz oscillator, we took  $\epsilon_s = 11.7045$ ,  $\omega_0 = 1.1406 \times 10^{16}$  rad/s,  $\hat{\omega}_0 = 1.0995 \times 10^{15}$  rad/s,  $\gamma_0 = 3.802 \times 10^8 \text{ s}^{-1}$ . Such values mimic the dispersion relation of  $\text{Al}_{0.1}\text{Ga}_{0.9}\text{As}$ , yielding an effective index  $n = 3.3258$  at  $\lambda = 1.55 \mu\text{m}$  [19]. Finally, we chose  $P_0 = 1$  ( $\text{C}/\text{m}^2$ ) to get a Kerr coefficient  $n_2 \simeq 10^{-18}$  ( $\text{m}^2/\text{W}$ ), as determined by evaluating self phase modulation by numerical integration of (1). The latter is a conservative value if compared to  $n_2$  in polymers, liquid crystals, semiconductors [20–22].

### 3 Linear response

In order to infer the band structure of the PC-wire, we launched an SC pulse in the transverse-electric ( $y$ ) linear polarization. Such pulsed input encompasses a broad spectrum; hence, it can excite all the modes with compatible symmetry features. After excitation, the  $y$ -component of the electric field ( $E_y$ ) was acquired in both D1 and D2 and Fourier transformed to yield the spectra of Fig. 2. In either positions within the wire a sharp band-gap is visible and centered around  $\lambda = 1500$  nm, owing to the chosen ratio  $r/a$ . The stars above the top panel in Fig. 2 mark three wave-

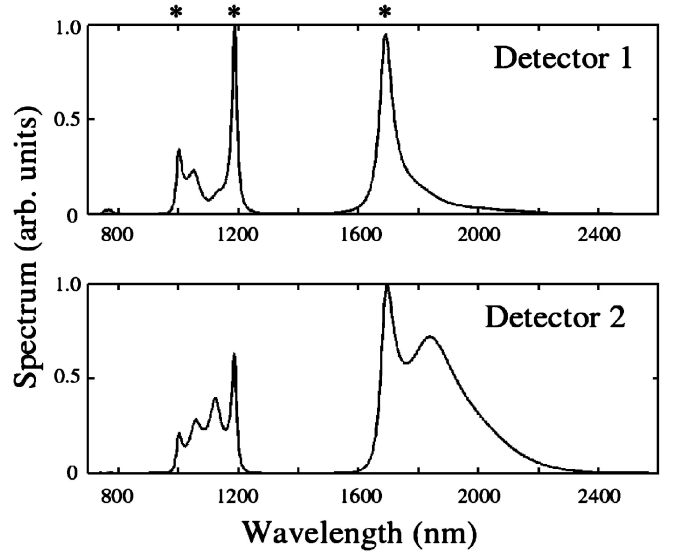


**FIGURE 2** Normalized spectra obtained in D1 (*upper panel*) and D2 (*lower panel*) by taking the square moduli of the Fourier transforms of the electric field

lengths  $\lambda_1 = 1 \mu\text{m}$ ,  $\lambda_2 = 1.118 \mu\text{m}$ ,  $\lambda_3 = 1.695 \mu\text{m}$  at which we performed numerical experiments to characterize the device transmission. To this extent we carried out simulations with cw excitations to visualize the field ( $E_y$ ) distribution and symmetry, as shown in Figs. 3 throughout 5 corresponding to cross-sections  $yz$  in  $x = L_x/2$  (a) and  $xz$  in  $y = L_y/2$  (b), respectively. The limited number of holes does not allow for

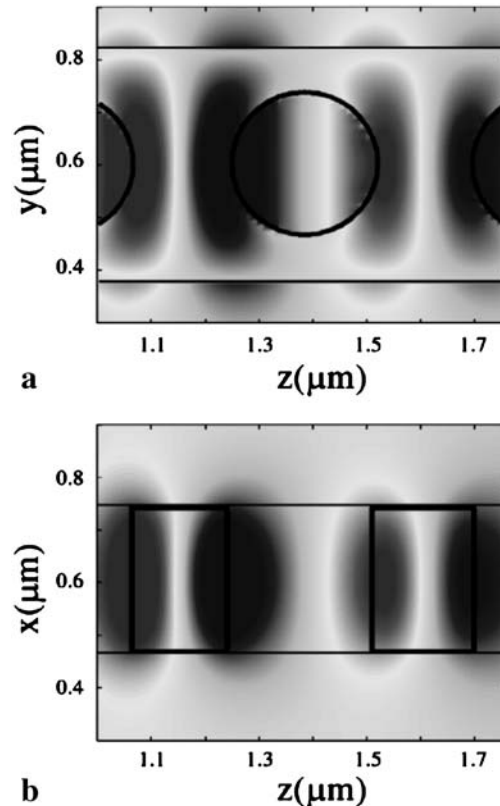


**FIGURE 3**  $y$ -component of the electric field for  $\lambda = 1 \mu\text{m}$ . **a**  $E_y$  in the  $yz$  plane; **b**  $E_y$  in the  $xz$  plane

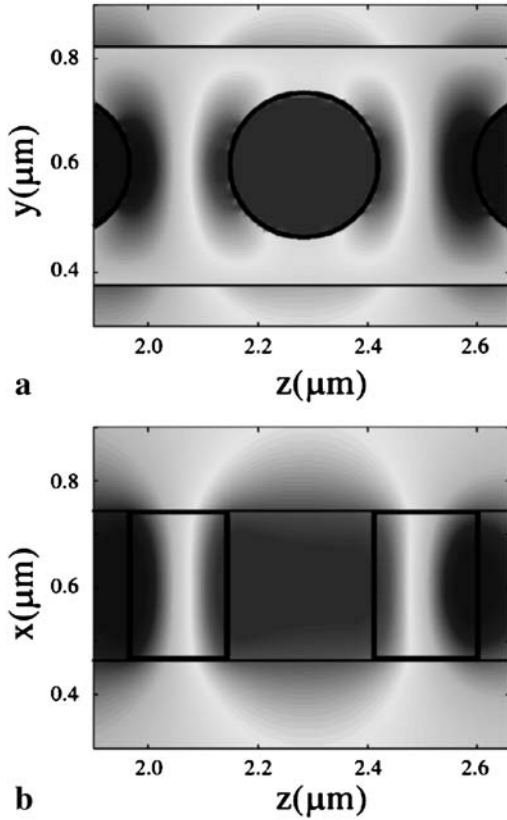


FIGURE 4  $y$ -component of the electric field for  $\lambda = 1.186 \mu\text{m}$ . **a**  $E_y$  in the  $yz$  plane; **b**  $E_y$  in the  $xz$  plane

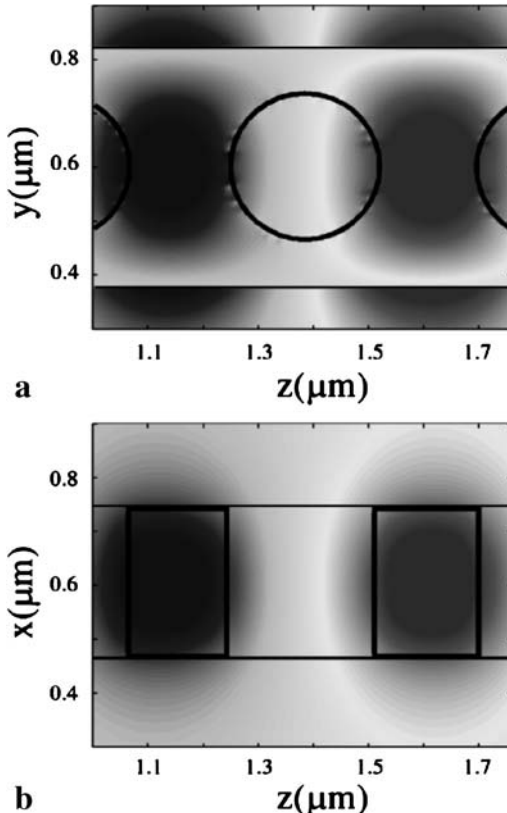


FIGURE 5  $y$ -component of the electric field for  $\lambda = 1.695 \mu\text{m}$ . **a**  $E_y$  in the  $yz$  plane; **b**  $E_y$  in the  $xz$  plane

the application of a standard frequency analysis; however, this field mapping enables us to characterize the excited modes at the wavelengths of interest and where the electric field is mainly localized. The differing spatial distributions (at  $\lambda_1$ ,  $\lambda_2$  and  $\lambda_3$ ) correspond to unequal excitability and transmission of the wire. Feeding the PC at  $\lambda_1$ , the transverse electric field shows maxima and minima well distributed among air (holes) and the medium, in both the horizontal (Fig. 3a) and the vertical (Fig. 3b) sections.  $\lambda_1$ , in fact, lies well outside the band-gap displayed in Fig. 2. At  $\lambda_2$ , conversely, the pump is located at the high PC band-edge (in frequency):  $E_y$  is more intense in the empty portions of the structure (Fig. 4). The opposite case is displayed in Fig. 5 with reference to a pump wavelength ( $\lambda_3$ ) at the lower band-edge: the field is mostly localized within the medium. To calculate the low-power (linear) transmission, we launched  $P_{\text{in}} = 1 \text{ W}$  in the feeding waveguide for the three cases above, and obtained  $T(\lambda_1) = 21.3\%$ ,  $T(\lambda_2) = 51\%$ ,  $T(\lambda_3) = 97\%$ , respectively, for the ratios between output (e.g. in D2) and input powers. Such limited values originate from the impedance mismatch between guided-wave and PC- modes, inevitable when a uniform waveguide is attached to a periodic structure [23–25].

The  $Q$ -factors of each involved mode need also be taken into careful consideration. However, it is hardly useful to calculate the unloaded  $Q$ 's, as often evaluated in literature by exciting the resonant mode with a proper intra-cavity source. This approach, in fact, does not provide a sound estimate of the actual device response when supplying energy from outside, as it would be in most real applications. Therefore, we evaluated the loaded  $Q$ -factors, inclusive of coupling and radiation losses.

By fitting the excitation time with the function of  $1 - \exp[-(\omega_0/2Q)t]$ , we computed  $Q_1 = 20$ ,  $Q_2 = 28$ ,  $Q_3 = 15$  at the three wavelengths, respectively, in good agreement with the existing literature [14, 26, 27]. As anticipated above, such differing  $Q$ 's (and  $T$ 's) relate to the unequal spectra gathered in D1 and D2 for the same excitation (see Fig. 2).

#### 4 Nonlinear dynamics

The main idea behind a PC optical parametric oscillator (OPO) stems from the large pump fluencies available in the micro-cavity. The energy can then be re-distributed via FWM between all the Bloch modes of the structure, with efficiencies depending on symmetry constraints and  $Q$ -factors of both pump and modes. The coupled mode theory in the time domain, adopted in [28] to treat quadratic parametric oscillators, can be utilized for the study of parametric oscillations via degenerate FWM. The oscillation process is characterized by a threshold power, which depends on the  $Q$ 's of both the pump and the modes as:

$$P_{\text{th}} = \frac{\omega}{2|g|Q\sqrt{Q_+Q_-}}, \quad (2)$$

where the two generated frequencies  $\omega_+$  and  $\omega_-$  are such that  $2\omega = \omega_+ + \omega_-$  and  $Q_{\pm}$  are the corresponding quality factors, respectively.  $g$  is the relevant three-dimensional overlap integral between the modal field profiles and the spatial distribution of the nonlinearity. If enough power is made available, the newly generated frequencies play the role of

(secondary) pumps, and the PC density of states ([4]) will be reproduced in the output spectrum. To verify and explore such features, we performed simulations in cw increasing the power at the pump wavelengths already investigated in the linear regime. We achieved a spectral resolution  $\Delta f \simeq 1.11 \times 10^{12} \text{ s}^{-1}$  by recording the time-varying signals at the output (D2) for intervals as long as 900 fs. Figures 6 through 8 show the normalized square modulus of the Fourier transforms of the electric field  $|\mathcal{F}(E_y)|^2$ , at the output (log scale on the vertical axes) for the cases above, comparing linear ( $P_{\text{in}} = 1 \text{ W}$ ) and nonlinear ( $P_{\text{in}} = 2 \text{ kW}$ ) responses. It should be noted in passing that the power needed to observe oscillations not only depends on the  $Q$ -factors of the excited modes, but it also scales with the material  $n_2$ . As the pump wavelength is tuned, the OPO spectra markedly change, as apparent in the figures. Their widths are linked to the pertinent  $Q$ 's and the distribution of neighboring states, with higher  $Q$ 's corresponding to better light confinement in the resonator and, hence, more efficient nonlinear response and energy exchange via FWM. While the wavelength  $\lambda_1$

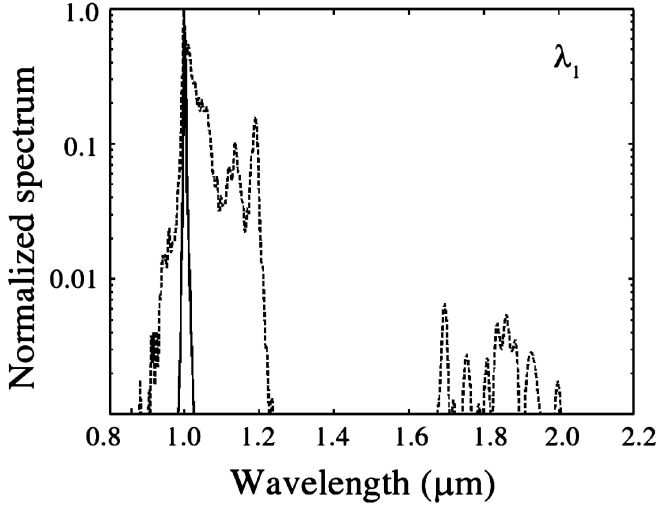


FIGURE 6  $|\mathcal{F}(E_y)|^2$  at the output of the wire (D2) for  $\lambda_1$  ( $Q \simeq 20$ ). Solid line:  $P_{\text{in}} = 1 \text{ W}$ ; dashed line:  $P_{\text{in}} = 2 \text{ kW}$

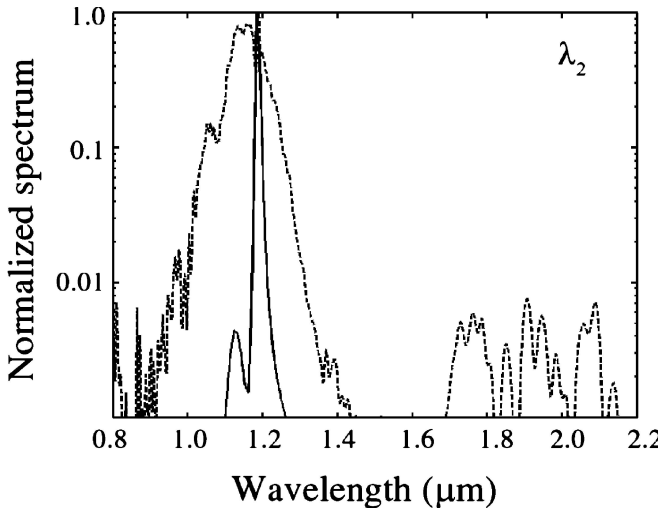


FIGURE 7  $|\mathcal{F}(E_y)|^2$  at the output of the wire (D2) for  $\lambda_2$  ( $Q \simeq 28$ ). Solid line:  $P_{\text{in}} = 1 \text{ W}$ ; dashed line:  $P_{\text{in}} = 2 \text{ kW}$

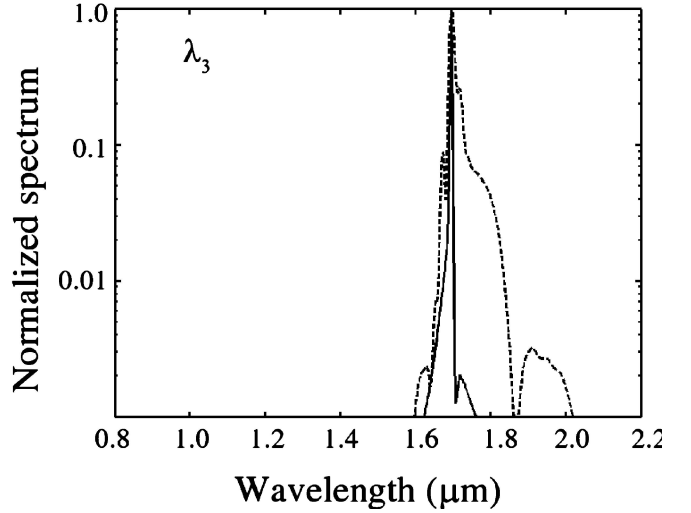


FIGURE 8  $|\mathcal{F}(E_y)|^2$  at the output of the wire (D2) for  $\lambda_3$  ( $Q \simeq 15$ ). Solid line:  $P_{\text{in}} = 1 \text{ W}$ ; dashed line:  $P_{\text{in}} = 2 \text{ kW}$

(with  $Q = 20$  and  $T = 0.21$ ) represents an intermediate behavior of the wire-OPO,  $\lambda_2$  (with  $Q = 28$  and  $T = 0.51$ ) yields a broader spectrum (Fig. 7) and  $\lambda_3$  ( $Q = 15$  and  $T = 0.97$ ) a narrow output which does not extend beyond the band-gap region (Fig. 8). In the latter case, in fact, the low  $Q$  penalizes the nonlinear response while allowing a better transmission.

Notice that the secondary peaks associated to the pump (solid line) in Figs. 7 and 8 at lower and higher frequencies, respectively, are due to the non-monochromatic “*mm*” excitation, the spectrum of which overlaps with other modes in the initial stage of the interaction.

## 5 Conclusions

We investigated optical oscillators based on four wave mixing in one-dimensional PC wires. To such an extent, we resorted to a fully parallelized three-dimensional FDTD code including material dispersion and a cubic nonlinearity. In this novel geometry we demonstrate that optical parametric oscillations can be efficiently obtained even in isotropic media encompassing a Kerr nonlinear response. The interplay between resonant, dispersive and nonlinear properties in such PC-wires links the mode excitation to the pertinent quality factors and the overall transmission. The ease of tailoring both these aspects in PC-wires is a key factor in obtaining a good tunability of the OPO with pump power, and underlines the relevance of proper trade-offs in the device design.

These results stress the richness afforded by photonic crystals in enhancing resonant nonlinear interactions, and pave the way to an entire new generation of highly integrated optical parametric sources where a careful design could compensate a limited nonlinearity.

**ACKNOWLEDGEMENTS** We acknowledge partial support from INFN-Initiative Parallel Computing, the Tronchetti-Provera Foundation and the Italian Electronic and Electrical Association (AEI). We thank Prof. S. Riva Sanseverino (University of Palermo) for enlightening discussions.

## REFERENCES

- 1 S. John: Phys. Rev. Lett. **58**, 2486 (1987)
- 2 E. Yablonovitch: Phys. Rev. Lett. **58**, 2059 (1987)
- 3 J.D. Joannopoulos, P.R. Villeneuve, S. Fan: *Photonic Crystals* (Princeton University Press, Princeton 1995)
- 4 K. Sakoda: *Optical Properties of Photonic Crystals* (Springer Verlag, Berlin 2001)
- 5 R.D. Meade, A. Devenyi, J.D. Joannopoulos, O.L. Alerhand, D.A. Smith, K. Kash: J. Appl. Phys. **75**, 4753 (1994)
- 6 C. Conti, S. Trillo, G. Assanto: Phys. Rev. Lett. **85**, 2502 (2000)
- 7 S.F. Mingaleev, Y.S. Kivshar: J. Opt. Soc. Am. B **19**, 2241 (2002)
- 8 M.F. Yanik, S. Fan, M. Soljačić: Appl. Phys. Lett. **14**, 2739 (2003)
- 9 J.S. Foresi, P.R. Villeneuve, J. Ferrera, E.R. Thoen, G. Steinmeyer, S. Fan, J.D. Joannopoulos, L.C. Kimerling, H.I. Smith, E.P. Ippen: Nature **390**, 143 (1997)
- 10 O. Painter, R.K. Lee, A. Scherer, A. Yariv, J. D. O'Brien, P.D. Dapkus, I. Kim: Science **284**, 1819 (1999)
- 11 A. Blanco, E. Chomski, S. Grabtchak, M. Ibsate, S. John, S.W. Leonard, C. Lopez, F. Meseguer, H. Miguez, J.P. Mondia, G.A. Ozin, O. Toader, H.M. Van Driel: Nature **405**, 437 (2000)
- 12 J. Vučković, M. Lončar, H. Mabuchi, A. Scherer: IEEE J. Quantum Electron. **QE-38**, 850 (2002)
- 13 H.Y. Ryu, M. Notomi, Y.H. Lee: Phys. Rev. B **68**, 045209 (2003)
- 14 J.P. Zhang, D.Y. Chu, S.L. Wu, W.G. Bi, R.C. Tiberio, R.M. Joseph, A. Taflove, C.W. Tu, S.T. Ho: IEEE Photon. Technol. Lett. **8**, 491 (1996)
- 15 J. Koga: Opt. Lett. **24**, 408 (1999)
- 16 J.L. Young, R.O. Nelson: IEEE Antennas Propagat. Mag. **43**, 61 (2001)
- 17 A. Taflove, S.C. Hagness: *Computational Electrodynamics: the FDTD method* (Artech House, London 2002)
- 18 R.R. Ziolkowsky, E. Heyman: Phys. Rev. E **64** 056625 (2001)
- 19 M.A. Afromovitz: Solid State Commun. **15**, 59 (1974)
- 20 M.B. Marques, G. Assanto, G.I. Stegeman, G.R. Mohlmann, E.W.P. Erdhuisen, W. Horsthuus: Appl. Phys. Lett. **58**, 2613 (1991)
- 21 I.C. Khoo: *Liquid crystals: Physical Properties and nonlinear Optical Phenomena* (Wiley, New York 1995)
- 22 J.A. Aitchison, D.C. Hutchings, J.U. Kang, G.I. Stegeman, A. Villeneuve: IEEE J. Quantum Electron. **QE-33**, 341 (1997)
- 23 R.E. Collin: *Field Theory of Guided Waves* (Oxford University Press, Oxford 1990)
- 24 S. Boscolo, C. Conti, M. Midrio, C.G. Someda: IEEE J. Lightwave Technol. **20**, 304 (2002)
- 25 A.S. Jugessur, P. Pottier, R.M. De La Rue: Electron. Lett. **34**, 367 (2003)
- 26 P.R. Villeneuve, S. Fan, J.D. Joannopoulos: Phys. Rev. B **54**, 7837 (1996)
- 27 D.J. Ripin, K.Y. Lin, G.S. Petrich, P.R. Villeneuve, S. Fan, E.R. Tohen, J.D. Joannopoulos, E.P. Ippen, L.A. Kolodziejski: IEEE J. Lightwave Technol. **17**, 2152 (1999)
- 28 A. Yariv, W. Louisell: IEEE J. Quantum Electron. **QE-2**, 418 (1996)